ARL-TR-10004 ● Oct 2024

Investigation of the Role of Temperature in Shock-Induced Initiations of Explosives Using an Ultrafast Indirect Laser Heating Technique

by Nhan C Dang, Jennifer L Gottfried, and Frank C De Lucia Jr

NOTICES

Disclaimers

The findings in this report are not to be construed as an official Department of the Army position unless so designated by other authorized documents.

Citation of manufacturer's or trade names does not constitute an official endorsement or approval of the use thereof.

Destroy this report when it is no longer needed. Do not return it to the originator.

ARL-TR-10004 ● OCT 2024

Investigation of the Role of Temperature in Shock-Induced Initiations of Explosives Using an Ultrafast Indirect Laser Heating Technique

Nhan C Dang, Jennifer L Gottfried, and Frank C De Lucia Jr
DEVCOM Army Research Laboratory

REPORT DOCUMENTATION PAGE

1. REPORT DATE	2. REPORT TYPE	3. DATES COVERED	
		START DATE	END DATE
October 2024	Technical Report	1 October 2023	30 September 2024

4. TITLE AND SUBTITLE
Investigation of the Role of Temperature in Shock-Induced Initiations of Explosives Using an Ultrafast Indirect Laser Heating Technique

5a. CONTRACT NUMBER	5b. GRANT NUMBER	5c. PROGRAM ELEMENT NUMBER
5d. PROJECT NUMBER	**5e. TASK NUMBER**	**5f. WORK UNIT NUMBER**

6. AUTHOR(S)
Nhan C Dang, Jennifer L Gottfried, and Frank C De Lucia Jr

7. PERFORMING ORGANIZATION NAME(S) AND ADDRESS(ES)
DEVCOM Army Research Laboratory
ATTN: FCDD-RLA-WA
Aberdeen Proving Ground, MD 21005

8. PERFORMING ORGANIZATION REPORT NUMBER
ARL-TR-10004

9. SPONSORING/MONITORING AGENCY NAME(S) AND ADDRESS(ES)	10. SPONSOR/MONITOR'S ACRONYM(S)	11. SPONSOR/MONITOR'S REPORT NUMBER(S)

12. DISTRIBUTION/AVAILABILITY STATEMENT
DISTRIBUTION STATEMENT A. Approved for public release: distribution unlimited.

13. SUPPLEMENTARY NOTES
ORCIDs: Nhan C Dang, 0009-0000-5752-8330; Jennifer L Gottfried, 0000-0002-1282-1928; Frank C De Lucia Jr, 0000-0003-2759-6978

14. ABSTRACT
The initiation of an explosive under shock loadings occurs in an extreme environment of high dynamic pressure and temperature (temperature jump, T-jump) on a rapid (picosecond) time scale. Within such a complex environment and brief transition time, the dynamic response of materials can be very difficult to observe and understand. Moreover, if the roles of pressure and temperature were better understood, our predictive capabilities for the dynamic response of materials would be dramatically improved, enabling the design of new molecules with the desired functionality. Therefore, determining the roles or functions of pressure and temperature is needed in the science of predictive capabilities for explosives. We are developing experimental techniques to determine the roles of T-jump and its behaviors in explosives under ultrafast heating. The heating is generated by inducing a T-jump in a transition metal film, a process that produces T-jump analogous to one that occurs in a shock-induced initiation. In this report, we present an overview of these techniques.

15. SUBJECT TERMS
indirect ultrafast laser heating, transient absorption, electronic excitations, temperature jump, Weapons Sciences

16. SECURITY CLASSIFICATION OF:			17. LIMITATION OF ABSTRACT	18. NUMBER OF PAGES
a. REPORT	b. ABSTRACT	C. THIS PAGE		
UNCLASSIFIED	UNCLASSIFIED	UNCLASSIFIED	UU	37

19a. NAME OF RESPONSIBLE PERSON	19b. PHONE NUMBER *(Include area code)*
Nhan Dang	(410) 306-0884

STANDARD FORM 298 (REV. 5/2020)
Prescribed by ANSI Std. Z39.18

Contents

List of Figures

List of Tables

1. Introduction

Shock and detonation physics seeks to predict how explosives will react in any given scenario. Predicting initiation requires a framework that includes a mechanism for the energy from an impact to couple into molecules. Experiments developed for the molecular time and length scales (i.e., picosecond and nanometer scales) are necessary to observe the subsequent dynamic response of materials under shock loading. However, due to the time and length scales, it is challenging to experimentally observe the dynamic behaviors and material responses of these materials. Furthermore, impact due to a shock event is a convolution of energies from the shock wave and temperature jump (T-jump), thus it is even more complicated to observe and interpret the behaviors and responses under shock loadings. Although a number of studies have been developed to characterize the reaction kinetics of millimeter- to centimeter-thick materials in second and sub-second time scales under T-jump,[1–6] at the molecular level no experiments have been made to directly investigate the role of T-jump. It is difficult to observe and understand the sole role of temperature at such a short time and length scale since the dynamic shock conditions—i.e., pressure, temperature and strain rate—can all be convolved into the material responses.

Of interest here is the role of T-jump in a shock-induced initiation, and the physical and chemical responses of materials under the influence of T-jump from the time that thermal energy couples into the sample to the time that chemical reaction occurs. A few theoretical and experimental studies have been done investigating thermal energy transfer from a flash-heated gold (Au) surface to adsorbed self-assembled monolayers (SAMs) using a flash thermal conductance (indirect flash heating) technique.[7–9] However, those studies focus on the thermal energy transport across the Au-sample interface; the vibrational transitions of specific SAM functional groups from molecules situated within a few carbon atoms of the Au surface were probed. We still need to understand the dynamic behaviors of thermal energy and the processes of thermal energy transfer in thicker samples for which the material responses under flash heating closely resemble those in the bulk material. Moreover, the chain of chemical reactions driven by the heat energy still needs to be determined.

Since ultrafast heating can travel up to approximately 10^3 nm/ps, obtaining 0.1-ps temporal resolution requires sensitivity to approximately 100 nm in the heated direction. These molecular processes are occurring on molecular time scales, so only femtosecond spectroscopies can observe these processes. To address the challenges mentioned above, we have been developing experimental tools to systematically investigate material responses under T-jump. In the early stages of

development, we have set up and developed indirect laser heating experiments coupled with femtosecond ultraviolet-visible (UV-VIS) transient absorption (TA) spectroscopy to investigate the physical and chemical responses of materials prior to chemical reaction. Next, we developed single-shot indirect laser heating experiments coupled with ultrafast mid-infrared (MIR) TA spectroscopy to observe dynamical changes in materials from the time of interacting with the heat energy to the start of the chemical reaction. In this report, we summarize the recent development and capabilities of these experiments.

2. Techniques

The indirect femtosecond laser heating technique used to generate the T-jump has been detailed elsewhere.[8,10] Here, for clarification, we describe the fundamental capabilities for observing the dynamic flow of thermal energy generated from T-jump in an Au film into explosives, and for probing physical and chemical responses of materials under heat loadings on the time scale of picoseconds. Overviews of the experimental setups are described below.

2.1 Sample Configurations

Solid and liquid samples are configured in multiple layers as illustrated in Fig. 1. Starting from left to right, the layers for the solid samples (Fig. 1a) are 500-μm sapphire substrate (Esco, not oriented), 110-nm Au film (vapor deposited on the back of the sapphire substrate), and approximately 5-μm-thick samples (deposited on the Au film surface using spin-coating technique). For liquid samples (Fig. 1b), the assembly (from left to right) consists of a 500-μm sapphire substrate (Esco, not oriented), 110-nm Au film (vapor deposited on the back of the sapphire substrate), approximately 50–100 μL of liquid sample pressed inside of a mylar spacer (Harrick Scientific: 6, 12, or 25 μm), and a 500-μm sapphire window (Esco, not oriented). Except when otherwise specified for particular studies, these sample configurations are used for each experiment.

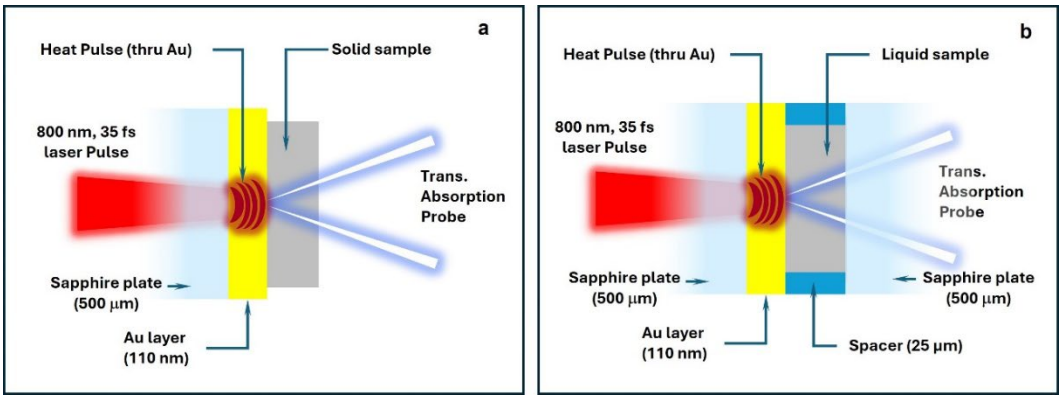

Fig. 1 Schematic diagrams of sample configurations for the experiments using the ultrafast indirect laser heating technique coupled with UV-VIS TA spectroscopy. a) Configuration for solid sample; b) configuration for liquid sample.

2.2 Heat Pulse Generation

A femtosecond laser pulse significantly enhances the energy density on target compared to other heating methods. It has been shown that during the very early laser-metal interaction in a transition-metal film, a nonequilibrium thermal state and a significant hot electron blast wave are generated in the metal film, leading to extremely high rates of electron temperature change and an initial compressive stress in the metals.[11–13] The temperature change that occurs due to the absorption of laser energy through electrons and lattice vibrations in the metal gives a sharp and strong rise of a short-lived (~10 ps) electron temperature (T_e) followed by a much lower and longer-lived (up to 1 ns) lattice temperature (T_l); $T_e = T_l$ when thermal equilibrium between electrons and the lattice is reached. Of interest here is a sharp and strong heat pulse that can generate T-jumps in materials analogous to those obtained during shock loadings. Among the transition metals, Au has been identified to produce the sharpest and strongest T_e under ultrafast laser interaction, making it the best choice to generate heat pulses in our experiments.

The basic principle of a laser pulse amplification in the regeneratively amplified stage of a femtosecond laser system is summarized in Fig. 2. In this stage, first, the input pulse is temporally stretched out using a dispersive delay line (stretcher) and then amplified to saturation with a high-power solid-state laser. At this step, the pulse is called a “chirped pulse” in which laser frequencies are stretched out in time, i.e., the light for each laser frequency arrives at a different time. In the final step of this stage, the pulse is recompressed using an inverse delay line (compressor) to obtain a high-peak-power laser pulse. Using the chirped and recompressed pulses, we can generate long- and short-lived heat pulses, respectively.

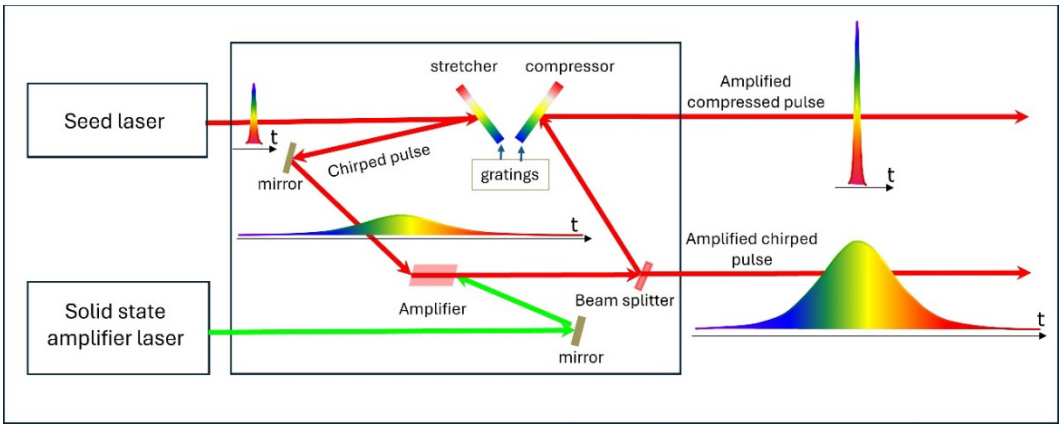

Fig. 2 Schematic diagrams of the laser pulse amplification in the regeneratively amplified stage of a femtosecond laser system

During heating, Au strongly absorbs UV-VIS light in the range from 375 to 650 nm. In the experiment utilizing UV-VIS TA spectroscopy coupled with the indirect ultrafast heating technique, a short-lived heating pulse is used to allow us to temporally resolve the UV-VIS TA signal of the Au film from the UV-VIS signal of the sample deposited on the Au since it occurs later in time. In terms of TA signal intensity, Fig. 3a illustrates a typical heat pulse with a pulse full width at half max of 3.5 ps and a rise time of 1.5 ps generated by a temporally compressed laser pulse with a width of 35 fs and an energy density of 15 mJ cm^{-2} on a 110-nm Au film. Figure 3b represents time-resolved TA signals of the Au surface and octahydro-1,3,5,7-tetranitro-1,3,5,7-tetrazocine (HMX) on the Au surface. The upper panel compares the time-resolved TA of Au (curve B) to that of HMX on the Au film (curve A) at 525 nm, while the low panel depicts the time-resolved TA of HMX (curve C), which is the difference of curves A and B. From the comparison, one can see that maximum TA of HMX starts at 9 ps, the time at which the heat propagates throughout the sample thickness. Therefore, the narrow heat pulse is necessary to temporally resolve the sample signal from that of the Au film in our current experiments.

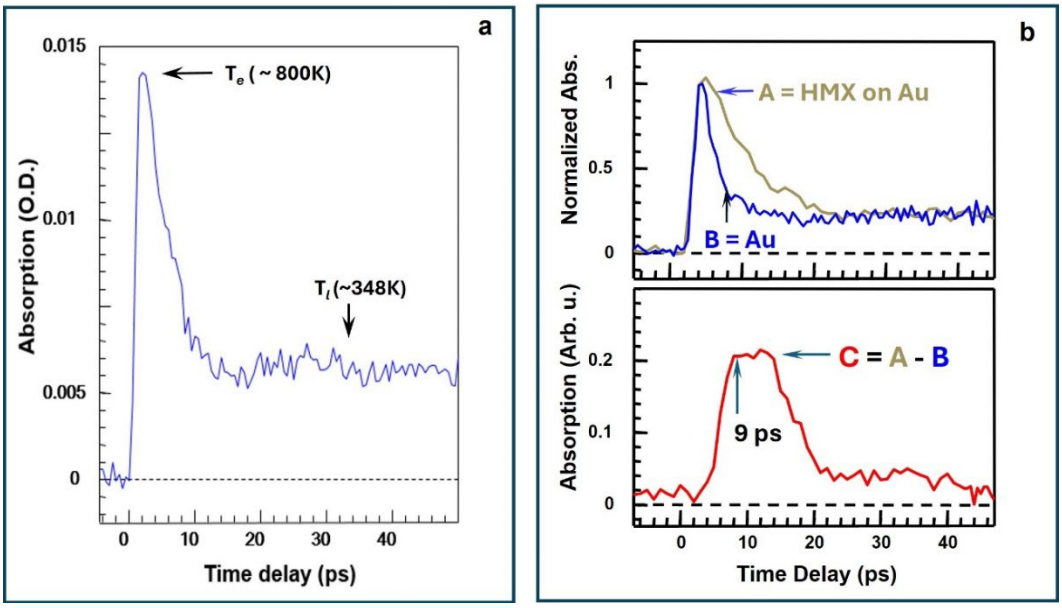

Fig. 3 a) Time-resolved transient absorption intensity profile at 525 nm of 110-nm Au film. b) A comparison of time-resolved transient absorption intensity profile at 525 nm of 110-nm Au film and HMX deposited on the Au film. Both samples were heated with a 35-fs laser pulse with an energy density of 15 mJ cm^{-2}.

2.3 Ultrafast UV-VIS TA Spectroscopy Coupled with Indirect Laser Heating Technique

Figures 4 shows the TA experimental scheme coupled with the indirect ultrafast heating technique. In this figure, a 3-mJ, 1-kHz rep rate compressed laser (Coherent Astrella) pulse train centered at approximately 800 nm with a pulse width of 35 fs is split (by a 80:20 beamsplitter) into two beam paths. The 80% beam is directed through a 125-mm focal lens and focused (through the sapphire window of a sample substrate) on the Au film (at the sapphire-Au film interface) to produce the heat pump. Upon contact, the laser pulse generates heat on the back side of the Au layer. The heat then travels through the Au layer and transfers into the sample. To prevent ablation of the Au layer or the formation of a laser-induced plasma on the Au surface, the laser energy density is attenuated by adjusting the laser energy and laser beam size (or adjusting focal length of the lens) such that the maximum laser energy density resulted in no visible damage to the Au surface.

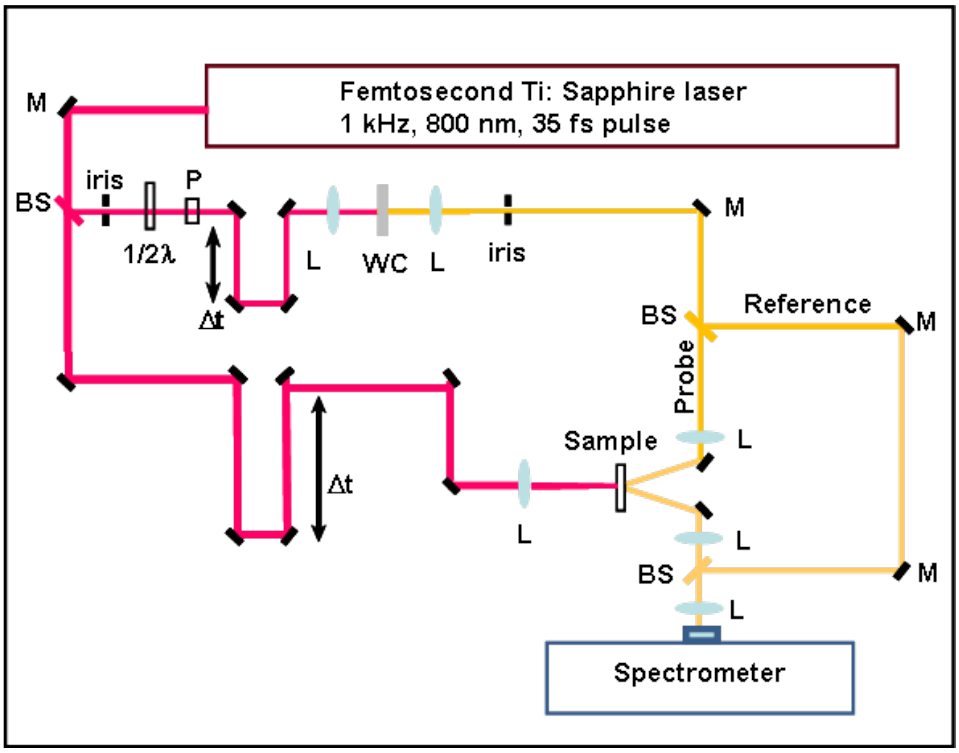

Fig. 4 Schematic diagram of the indirect laser heating with white light transient absorption spectroscopy experiment. Key: M = mirror; BS = beamsplitter; L = lens; P = polarizer; 1/2 λ = half-wave plate; Δt = time delay translational stage; WC = water cell.

For the second beam path, a small portion of the 20% beam is directed to focus onto a 3-mm-thick calcium window using a 150-mm focal length lens to generate a white light (WL) supercontinuum. To obtain a stable WL spectrum, the beam size, focal length, and energy of the input 800-nm laser beam are optimized such that nonlinear interactions within the window are minimal. The WL was then re-collimated with a 150-mm focal length lens. The beam is further spatially filtered by an iris to obtain the most stable and intense WL. The WL was then split into probe and reference beams by a 50:50 beamsplitter. The probe beam is focused on the sample with an external angle of incidence of 30° and a spot size of 20 μm. The reflected probe and reference pulses are focused with a 75-mm focal length lens through a 100-μm slit and into an imaging spectrometer. The probe and reference intensities are then simultaneously recorded by an electronically gated CCD camera.

2.4 Data Acquisition

The timing for the WL supercontinuum and the heat pulse is determined in two steps. First, the temporal overlap of the heat pump laser pulse and the WL supercontinuum is determined using optical pump−probe transient absorption in a 6-μm-thick silicon (Si) single crystal. The absorption edge of Si is sufficiently close to the pulse wavelength at 800 nm to allow the 800-nm heat pump laser to be used

as the optical pump, and the long wavelengths of the supercontinuum are used as the probe. A photodiode with a filter blocking the 800-nm pump scatter monitored the supercontinuum intensity while the time delay between the pump and supercontinuum is scanned. The supercontinuum transmission dropped when the sharply rising initial edge of the pump pulse arrives. The time-zero delay between the supercontinuum and the pump laser pulse was determined at the initial drop of supercontinuum intensity. Next, to determine time-zero at which the heat pulse enters the sample—the time-zero delay at the Au-sample interface—transient absorption of the Au surface (before the samples are deposited) under the heat pump is used. Time-zero delay is determined at which the initial transient absorption signal appears when initial edge of the heat pulse (generated by the laser pulse interact in the Au film) arrives.

To measure TA, the percentage of the transient reflectance of probe pulses from the sample at various delay times relative to the heat pulse (determined by the delay line position) is recorded with a time resolution of 0.5 ps and calculated by the following equation:

$$R = \left[\frac{R_{pump\ on}}{Reference} - \frac{R_{pump\ off}}{Reference}\right] / \frac{R_{pump\ off}}{Reference} \quad (1)$$

where $R_{pump\ on}$ and $R_{pump\ off}$ are the reflectance recorded during and before heat, respectively. The probe intensity spectrum was normalized with respect to the reference for the same probe pulse to account for any fluctuations during measurements.

Absorbance was then calculated by

$$A = -\log(R + 1) \quad (2)$$

In general, to improve the signal-to-noise ratio, 50 transient absorption spectra at each time delay are obtained at each probed sample spot. Each final reported spectrum is an average of 150 spectra recorded at three different sample spots.

3. Capabilities and Potentials

3.1 Heat Propagation

Investigating propagation of the heat energy from T-jump through the sample and determining the propagation rate are the first steps required to verify whether a T-jump contributes to the chain reactions that occur during shock-induced initiation. We used the ultrafast indirect laser heating coupled with UV-VIS TA spectroscopy to observe the dynamic flow of the heat energy (from a T-jump

generated in an Au film) traveling through thin films of samples deposited on the Au film. In this section, the methods of determining heat propagation and propagation rate in explosives are described and discussed.

3.2 Two-Step Measurements

Figures 5 and 6 summarize the experimental schemes for two-step measurements for determining the propagation times (Δt) of heat pulses that propagate through thin films of solid and liquid samples, respectively, where $\Delta t = t_2 - t_1$; t_1 and t_2 are the time marks of heat entering at one boundary and arriving at the other boundary of the sample film. Figures 5a and 6a show the sample configurations of the first step measurements where time t_1 at surface 1 of the Au film 1 (thickness =110 nm) is determined using time-resolved UV-VIS TA of Au under heating from a 35-fs laser pulse centered at 800 nm and an energy density of 15 mJ cm^{-2}. Time t_1 was marked at maximum TA intensity of the Au film. Figures 5b and 6b depict the second step measurements in which the samples are sandwiched between two Au films, 1 and 2. Note that for a solid sample, to obtain absolute contact to the Au surfaces, the sample is spin coated onto Au surface 1, then a 20-nm-thick Au film (surface 2) is vapor deposited directly onto the sample. For a liquid sample, Au is vapor deposited onto sapphire substrates, and a spacer of known thickness is placed onto one of the Au surfaces. The liquid sample fills the volume created by the spacer, and the second Au-coated substrate is then pressed against the spacer with the Au surface adjacent to the sample. Time-resolved UV-VIS TA spectroscopy is again used to detect the TA of Au at the surface 2 of the Au film 2. A laser pulse is used as in step 1 to heat the Au–sample interface 1. Heat generated in Au interface 1 propagates through the sample film to arrive at the sample–Au interface 2 and heats Au film 2 where the TA signal of the Au film 2 is detected at time delay t_2. The maximum TA signal of the Au surface 2 at a time delay t_2 is marked. The heat propagation rate R is calculated by Eq. 3:

$$R = \frac{L}{\Delta t}, \tag{3}$$

where L is the sample thickness.

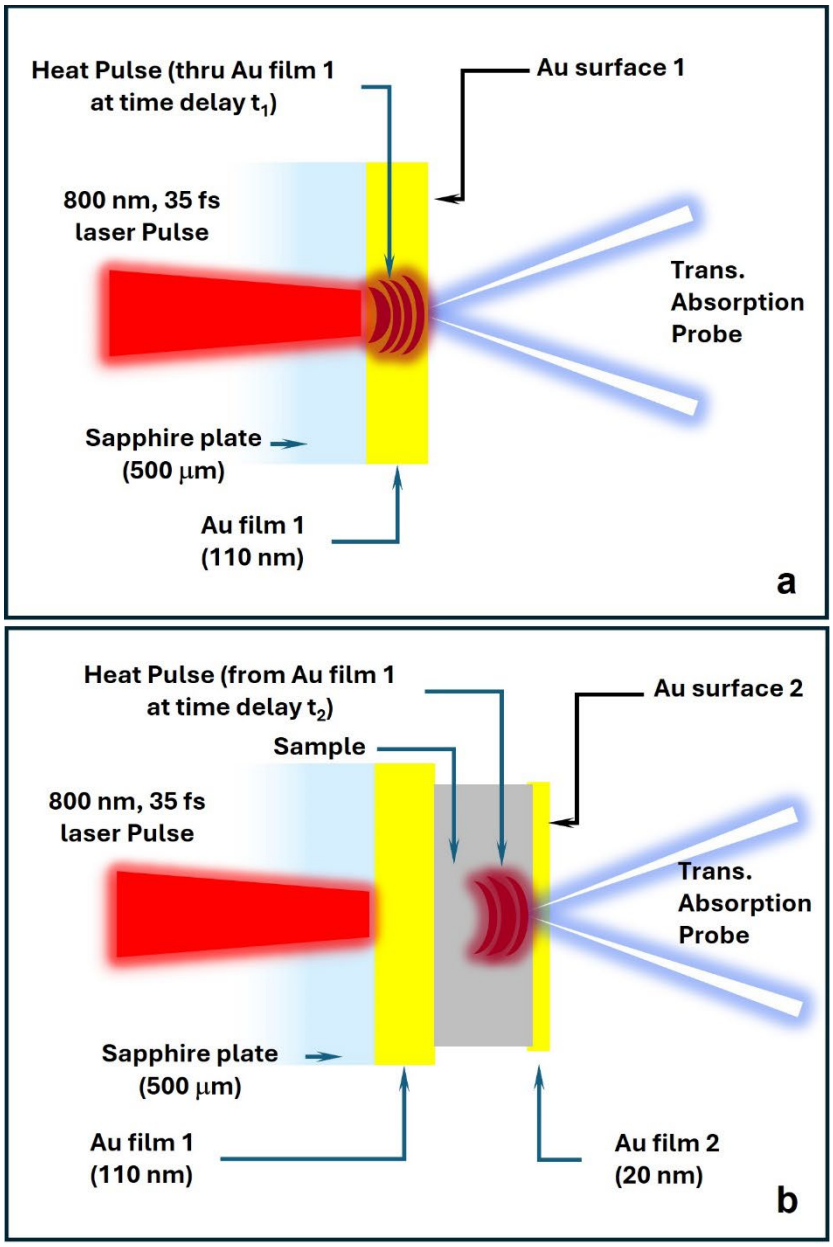

Fig. 5 Schematic diagrams of two-step measurements of heat propagating throughout a thin film of a solid sample using the ultrafast indirect laser heating technique coupled with UV-VIS TA spectroscopy. a) Experimental configuration for the first step, measuring heat propagation through the Au film (surface 1), and b) experimental configuration for the second step, measuring the heat propagation through a second Au film covering the sample (surface 2).

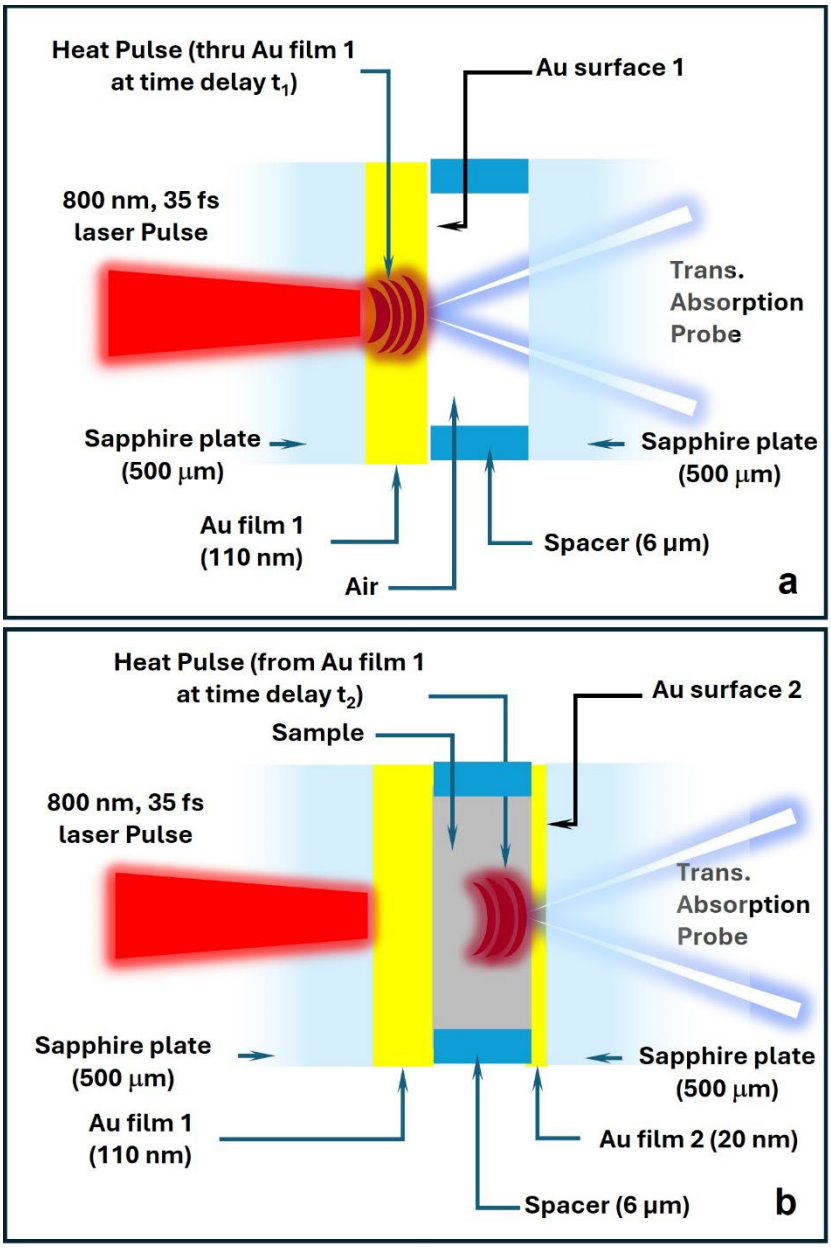

Fig. 6 Schematic diagrams of two-step measurements of heat propagating throughout a thin film of a liquid sample using the ultrafast indirect laser heating technique coupled with UV-VIS TA spectroscopy. a) Experimental configuration for the first step, measuring heat propagation through the Au film (surface 1), and b) experimental configuration for the second step, measuring the heat propagation through a second Au film covering the sample (surface 2).

Figure 7a shows how we obtained the measurement of Δt for heat propagating throughout a 6 ± 1 μm film of 1,3,5-trinitroperhydro-1,3,5-triazine (RDX). TA spectra of the Au surface 1 (upper panel) and Au surface 2 (lower panel) were measured as functions of time. Figure 6b shows the time-resolved TA intensity profile of the Au surface 1 (red curve) and Au surface 2 (blue curve) at 525 nm

from the first and second steps, respectively. Each curve is an average of five TA intensity profiles obtained with five different runs for each step. We used the maximum TA intensities in the time-resolved TA intensity profiles as reported in Fig. 6b to determine t_1 and t_2 and the calculated $\Delta t = 9 \pm 5$ ps. The heat propagation rate, therefore, is 0.67 ($\pm$ 0.48) $\times 10^6$ m/s calculated using Eq. 3.

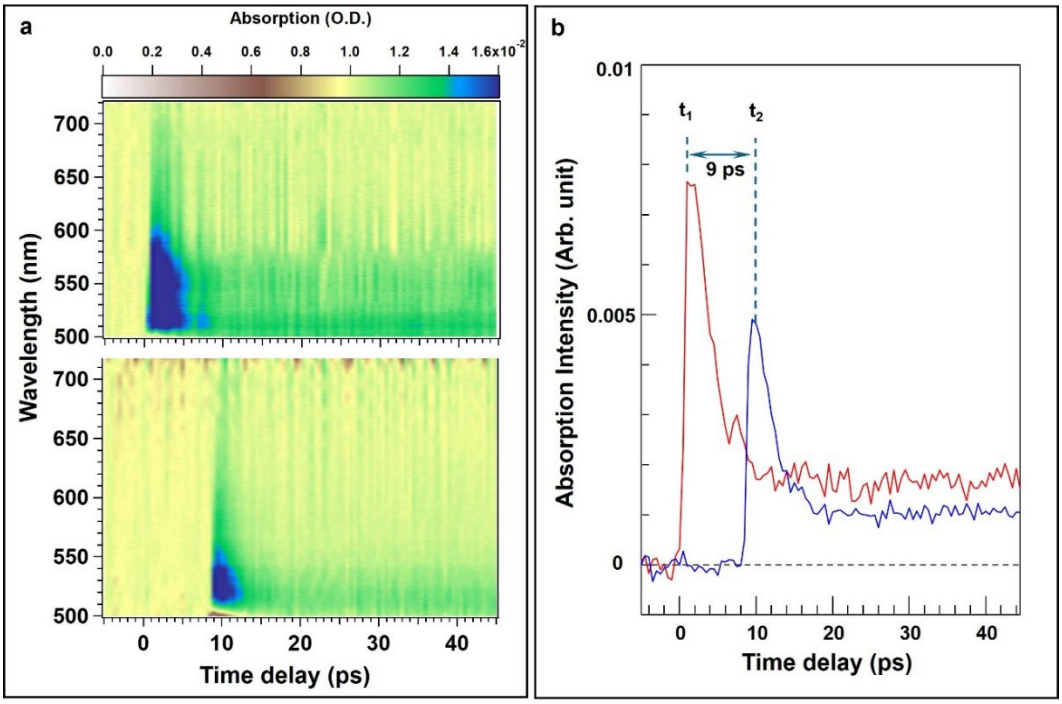

Fig. 7 a) Time-resolved TA of heated Au film 1 (upper panel) and 2 (lower panel) recorded using two-step measurements of heat propagation throughout a 6-μm RDX sandwiched between Au films 1 and 2. b) Time-resolved profiles of TA intensities at 525 nm of heated Au film 1 (red curve) and Au film 2 (blue curve). The time for the heat pulse to propagate through the thin RDX is determined by the time difference between the maximum absorption intensities of the two profiles (9 ps).

The measurement of propagation time between the two Au surfaces requires two separate experiments. The sample configuration used in the first experiment is modified for the second experiment. During the process of changing from one sample configuration (Fig. 5a or 6a) to another (Fig. 5b or 6b), micro- to sub-millimeter movement of the sample position (relative to the original position) is likely. This leads to the change of temporal and spatial overlaps of the pump and probe pulses, resulting in large experimental error of the time delay from one run to another.

3.3 One-Step Measurement

Eliminating the steps of reassembling and repositioning samples for experiments is necessary to obtain more accurate data. Figure 8a summarizes an experimental

scheme used to measure the time that heat propagates from Au surface 1 to Au surface 2 in one-step measurement. In this experiment, the sample is modified such that laser pulses can heat both Au surfaces simultaneously, and time-resolved UV-VIS TA is used to monitor both t_1 and t_2 at Au surface 2. To perform this task, the thickness of the first Au film is reduced so that the laser pulse can leak through and interact with the second Au layer simultaneously. The optimal parameters for the thickness of Au film 1 and the laser energy density that prevents ablation of the thinner Au film 1 are 50 nm and 10 mJ/cm^2, respectively. Figure 8b shows a time profile of the UV-VIS TA of the Au surface 2 at 525 nm for a 7.5 ± 1 μm film of RDX. The strong sharp TA signal at time t_1 is in response to the heat generated by the laser pulses at Au surface 2. The second TA signal at the time delay t_2 is in response to the heat generated by the heat pulse in Au film 1 propagating to and heating the Au film 2. Using t_1 and t_2, we determined a $\Delta t_{2\text{-}1}$ value of 15 ± 0.5 ps (note that 0.5 ps accounts for the error in the time resolution). Next, we used Eq. 3 to determine a heat propagation rate of 0.50 (±0.17) × 10^6 m/s, which agrees with the previous measured value of 0.67 (±0.48) × 10^6 m/s using the two-step method but has a smaller measurement error.

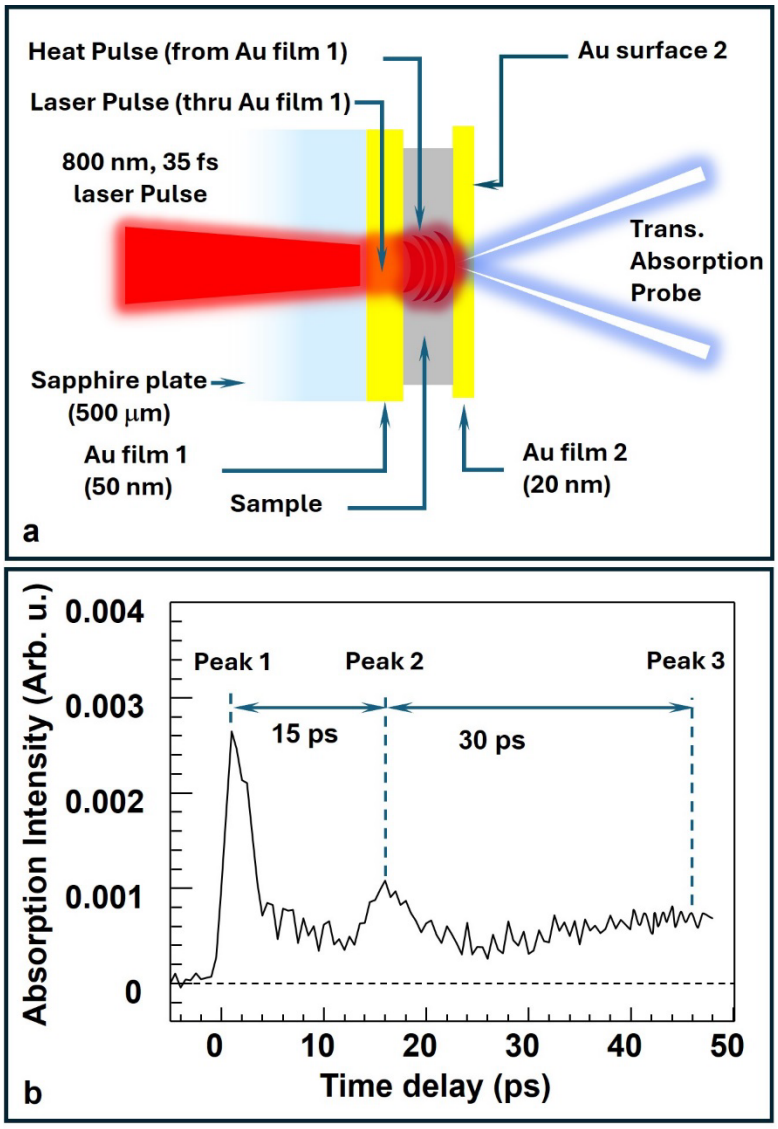

Fig. 8 a) Schematic diagrams of one-step measurements of time propagating throughout a thin film sample using the ultrafast indirect laser heating technique coupled with UV-VIS TA spectroscopy. b) Time-resolved profile of TA intensity at 525 nm of heated Au film 2. Time propagating throughout a thin RDX film (7.5 μm) is determined by the time difference between the maximum absorption intensities of peaks 1 and 2. Peak 1 depicts the time at which heat enters the first sample boundary (surface 1). Peak 2 depicts the time that heat arrives at the other end of the sample boundary (surface 2).

In Fig. 8b, it is observed that the TA signal at t_2 is temporally broader than the TA signal at t_1. The temporally broadened feature indicates the heat pulse is broadened at t_2. To explain the broadened heat pulse, we anticipate that there are two heat pulses simultaneously arriving at the Au film 2 at t_2. First, the heat pulse generated from the Au film 1 propagates throughout the sample and arrives at the Au film 2. Second, during the propagation a portion of the first heat pulse energy is stored (held up) in the sample lattice and heats up the sample, resulting in a lower

temperature but longer-lived heat pulse compared to the first one. Therefore, the heat pulse that arrives at t_2 is the result of a convolution of the first and second heat pulses, of which lower temperature but longer lifetime are expected as shown by the lower but temporally broader TA signal at t_2. Also, the low intensity and temporally broad TA signal at t_3 is observed. The TA signal at t_3 arises from the Au film 2 under heating of a heat pulse which is a convolution of the heat pulse arisen from the sample lattice and the reverberation of the original heat pulse reflected between the two sample boundaries interfaced with the two Au films. The time it takes for the heat at t_2 to propagate back to Au film 1 and then return to Au film 2 is $2 \times \Delta t_{2\text{-}1} = 30$ ps, and therefore at t_3, $\Delta t_{3\text{-}1} = 45$ ps.

Heat propagation in a 6-μm film of 2,4,6-triamino-1,3,5-trinitrobenzene (TATB) in dimethyl sulfoxide (DMSO) solution was investigated and compared to that obtained for RDX using the one-step measurement method. Figure 9a summarizes an experimental scheme used to measure the time of which heat propagates from Au surface 1 to Au surface 2 in one step measurement for the TATB in the DMSO sample using the same experimental parameters as the previous RDX experiment. Figure 9b depicts the heat propagation in the sample in terms of the time-resolved TA signal of Au surface 2 at 532 nm. Similar to RDX, a second temporally broad peak and the reverberation process (third peak) were observed in the TATB sample. The heat propagation rate was 0.92×10^6 m/s, and a temporally narrower band was observed at later times. The explanation for this is that since TATB in DMSO has lower electron–phonon coupling than that of RDX, it is not as efficient in storing heat energy in lattice, resulting in faster heat propagation and lower temperature arisen from the heat energy stored in the sample lattice. The heat pulse generated in Au film 1 maintains temperature as it propagates to Au film 2 compared to the heat pulse generated in RDX, as observed by the relative intensities of peak 2 to peak 1 in each experiment. Also, the second heat pulse generated in the sample lattice has a shorter lifetime indicated by the temporal width. As a result, the convolution of the two heat pulses in the TATB in DMSO sample has higher temperature and a shorter lifetime compared to that observed in RDX as seen in Fig. 8, where a lower and temporally broader TA signal is shown. More discussion of the dependency of heat transfer on electron–phonon coupling will be discussed in Section 3.5.

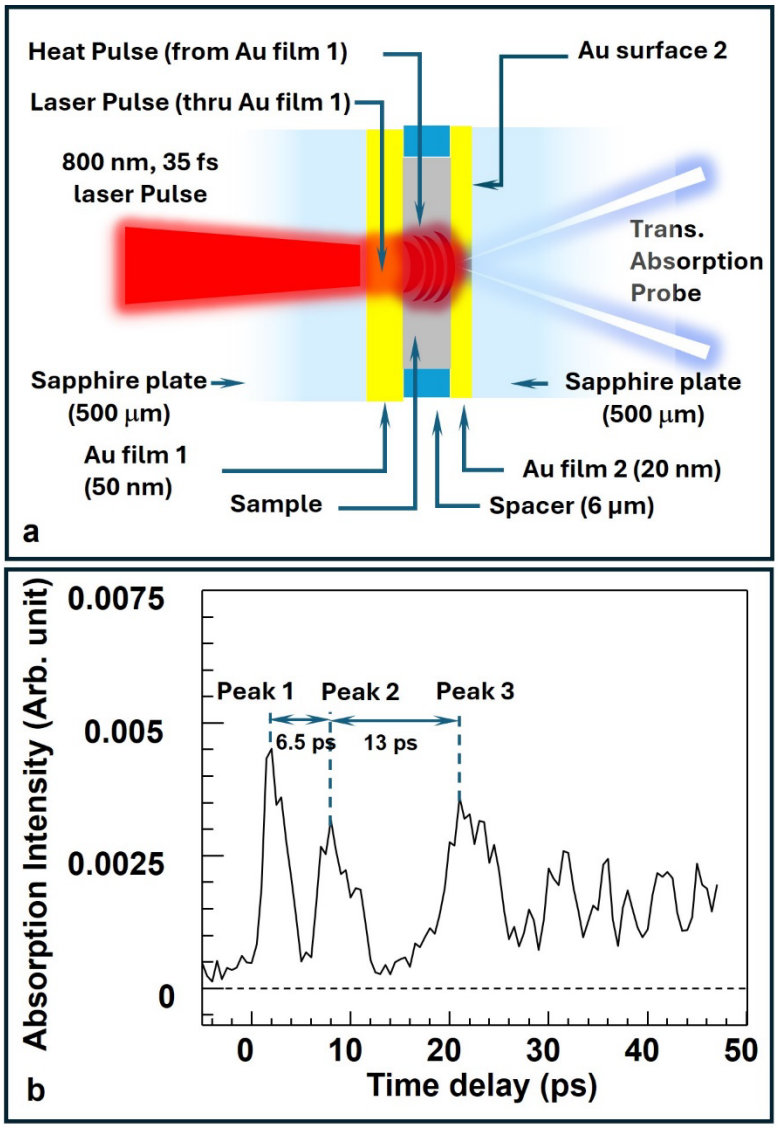

Fig. 9 a) Schematic diagrams of one-step measurements of time propagating throughout a 6-μm film of TATB in DMSO using the ultrafast indirect laser heating technique coupled with UV-VIS TA spectroscopy. b) Time-resolved profile of TA intensity at 525 nm of heated Au film 2. Peak 1 depicts the time at which heat enters the first sample boundary (surface 1). Peak 2 depicts the time that heat arrives at the other end of the sample boundary (surface 2). Time propagating throughout a thin RDX film (6 μm) is determined by the time difference between the maximum absorption intensities of peaks 1 and 2.

3.4 Heat Transfer

Understanding how and how fast heat energy propagating in the sample couples into molecules is the next step in determining the role of T-jump in the initial events of a shock-induced initiation. We successfully performed several studies to observe the process of heat energy coupling into the sample molecules using UV-VIS TA spectroscopy coupled with ultrafast indirect laser heating.[10,14–16] Here we

summarize the results that reflect how and how fast the thermal energy from T-jump couples into the explosive molecules from the studies of RDX, pentaerythritol tetranitrate (PETN), and HMX under heat pulses generated by the 35-fs laser pulses centered at 800 nm. Figure 10 displays the time-resolved TA spectra of Au, and RDX, HMX, and PETN on an Au surface. Compared to the TA of Au alone, additional TA is observed for RDX, PETN, and HMX, indicating that heat energy from T-jump transfers to and couples into the molecules by changing the electronic configurations of the molecules. The time-resolved TA intensities at 525 nm of these samples on Au compared to that of plain Au are shown in Fig. 11. By subtracting the time-resolved TA intensity of the Au layer from the time-resolved intensities of RDX, HMX, and PETN, we obtain the absorption difference spectra shown in the lower panel of Fig. 11. We observe that the sample absorptions start at approximately 2 ps and reach maximum at 9 ps in the 5-mm-thick samples. The findings indicate that it takes approximately 2 ps for the heat to couple into molecules and approximately 9 ps for the heat to propagate throughout the samples, indicated by the maximum TA signals.

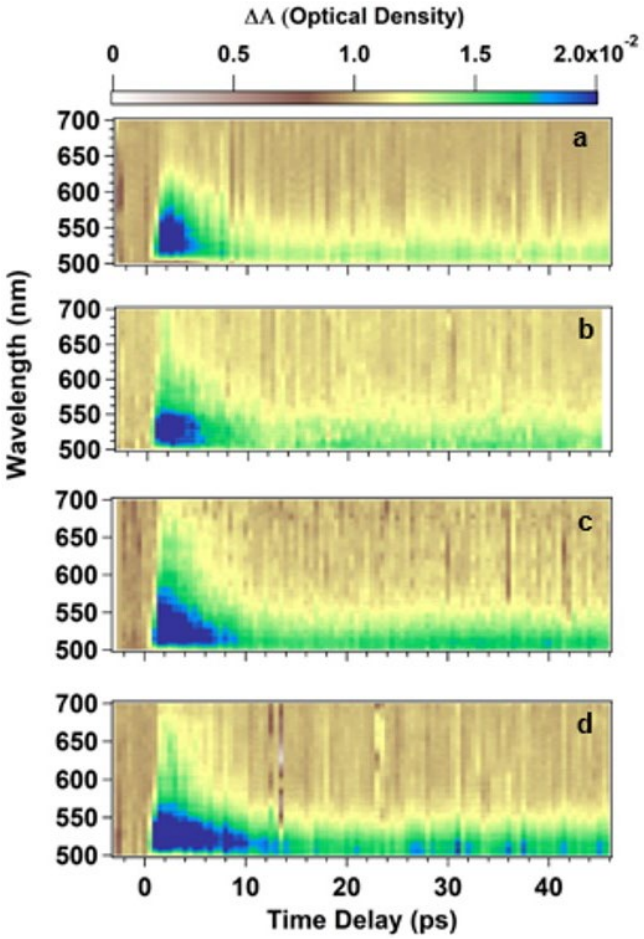

Fig. 10 2D time-resolved transient absorption spectra of heated thin films of a) Au, b) RDX on the Au film, c) PETN on the Au film, and d) HMX on the Au film

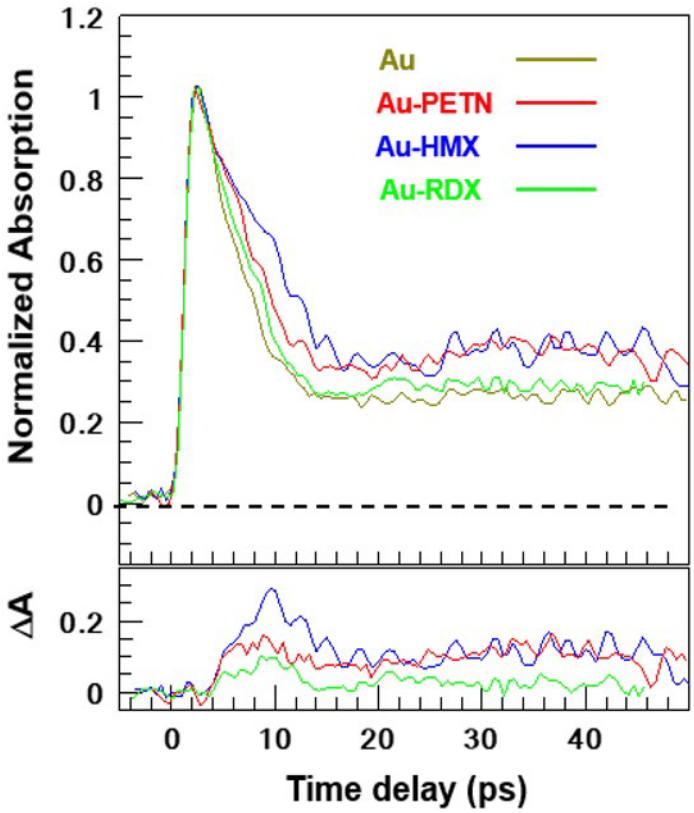

Fig. 11 Upper panel: time-resolved TA intensities of the Au film and RDX, PETN, and HMX films deposited on the Au layer. Lower panel: the differences between the TA intensity profiles of HMX, PETN, and RDX on Au and the Au layer.

3.5 Probing Physical Properties

Understanding the dependence of heat transfer on physical properties such as thermal conductivity, electron–phonon coupling, and morphology is essential for developing accurate models for explosive predictivity. In previous studies, using the ultrafast indirect laser heating coupled with UV-VIS TA spectroscopy, we were able to observe the dependency of heat transfer efficiency on material thermal conductivity, electron–phonon coupling, and morphology. Discussions of these findings are summarized below.

As shown in Fig. 11, among the three samples—RDX, PETN, and HMX—the strongest and weakest TA signals are observed for HMX and RDX, respectively. These observations are accordingly consistent with the thermal conductivity values of the three samples as seen in Table 1. The heat transfer will be more efficient through a sample with a higher thermal conductivity. Therefore, the stronger TA signal is observed for the sample with a higher thermal conductivity.

Table 1 Thermal conductivity of HMX, PETN, and RDX

Substances	Thermal conductivity ($\times 10^{-4} \frac{cal}{cm \cdot s \cdot C}$)
HMX	1.18
PETN	0.678
RDX	0.665

Electron–phonon coupling is another important factor that reflects energy transport in materials. As discussed by Hohlfeld et al.,[17] the energy transport is dependent on electron–phonon coupling in a material. Weaker phonon coupling in a material means less heat energy storage, therefore energy transport is faster. The results emphasize that electron–phonon coupling is an important factor in predicting heat energy transfer in an explosive. To study this, two improvements from our standard experiments are needed: 1) longer sustained heat energy is needed to support TA of the sample occurring in the lattice temperature, and 2) temporally resolved TA spectra between that of the metal surface and the sample deposited on the surface are necessary to determine the influence of the stored energy in the sample lattice.

To perform the improvements, the heat pulses are modified so that the TA signals of the metal surface are low, but the provided heat energy is high enough to produce and support TA signals of the sample beyond 10 ps at which the lattice temperature becomes important. Weak electron–phonon coupling found in Au allows the build-up of a high T_e and faster energy transport into deeper parts of the material. In contrast, strong electron–phonon coupling found in the transition metal platinum (Pt) retains much of the absorbed energy near the surface and produces slower energy transport into the sample, resulting in a lower T_e and a higher T_l. This generates enough heat energy to produce a TA signal of the sample that is strong and sustains long enough to distinguish from the TA signal of the Pt under the same heat pulse. By using a very thin film of Pt deposited between the interface of the Au and sample layers, we can obtain the two improvements discussed above.

Figure 12 shows sample configurations of the Au monolayer (a) and the Au/Pt bilayer (b) used to obtain heat pulses generated with a laser energy of 20 mJ/cm^2 as described by Dang et al.,[14] and comparisons of the heat pulses in term of TA intensity of the samples at 525 nm (c). Compared to the T_e and T_l generated in the Au monolayer (Fig. 12c, red curve), a significant decrease in T_e and increase in T_l is observed for the Pt/Au film (Fig. 12c, blue curve). Figure 13 shows the transient absorption spectra of 5-μm films of RDX and PETN on the Au/Pt bilayer under the heat pulse described above (Fig. 12). In Fig. 14, the strongest TA signal occurs within the first 5 ps for the Au/Pt surface (Fig. 13a) and the RDX sample (Fig. 13b) but is delayed until about 10 ps for PETN (Fig. 13c). The TA absorption for PETN

is also stronger at delay times longer than 10 ps. This observation suggests that compared to RDX, PETN more efficiently stores the thermal energy from the T-jump in the lattice. The findings suggest that electron–phonon coupling in PETN is stronger than that in RDX, and therefore stores more heat energy and couples more efficiently into PETN at later times.

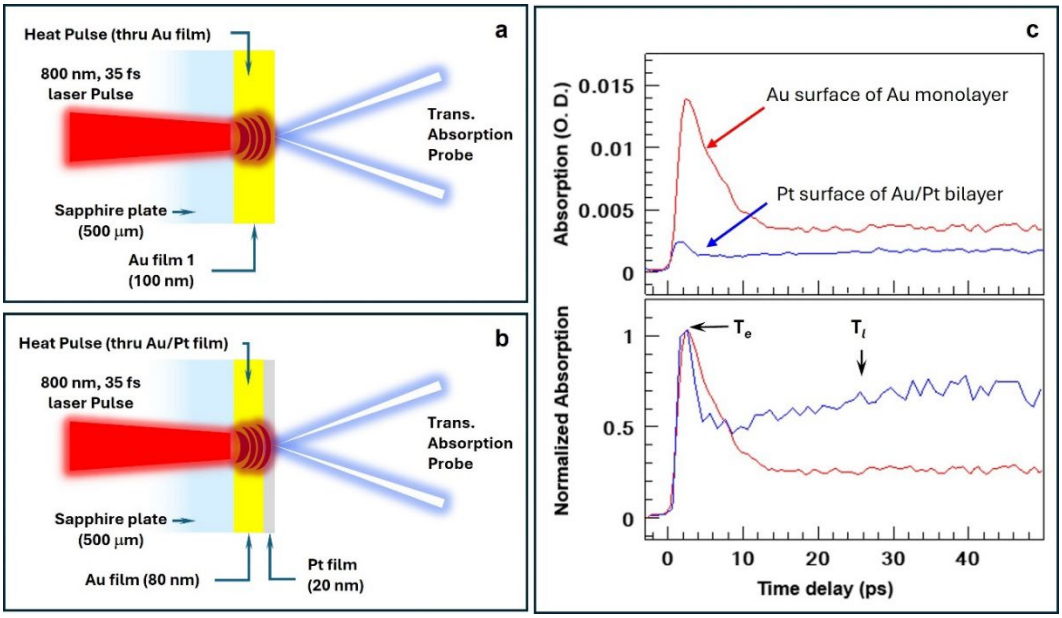

Fig. 12 Schematic diagrams of a) Au monolayer and b) Au/Pt bilayer used to generate heat pulses in Au and Au/Pt bilayer with an energy density of 20 mJ /cm^2. c) Heat pulses generated in Au monolayer and Au/Pt bilayer expressed in terms of absorption intensities (upper panel) and normalized absorption signals (lower panel) of Au surface of the Au monolayer and Pt surface of the Au/Pt bilayer at 525 nm as a function of time delay.

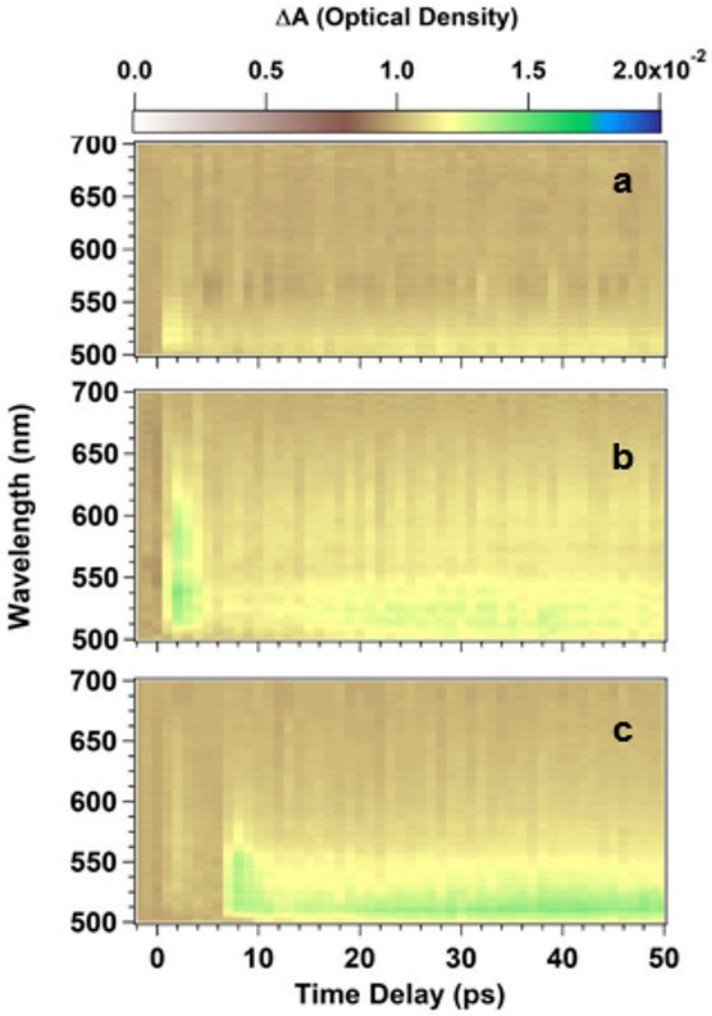

Fig. 13 2D time-resolved transient absorption spectra of materials a) Pt deposited on Au layer, b) RDX on the Pt surface of the Pt/Au bilayer, c) PETN on the Pt surface of the Pt/Au bilayer

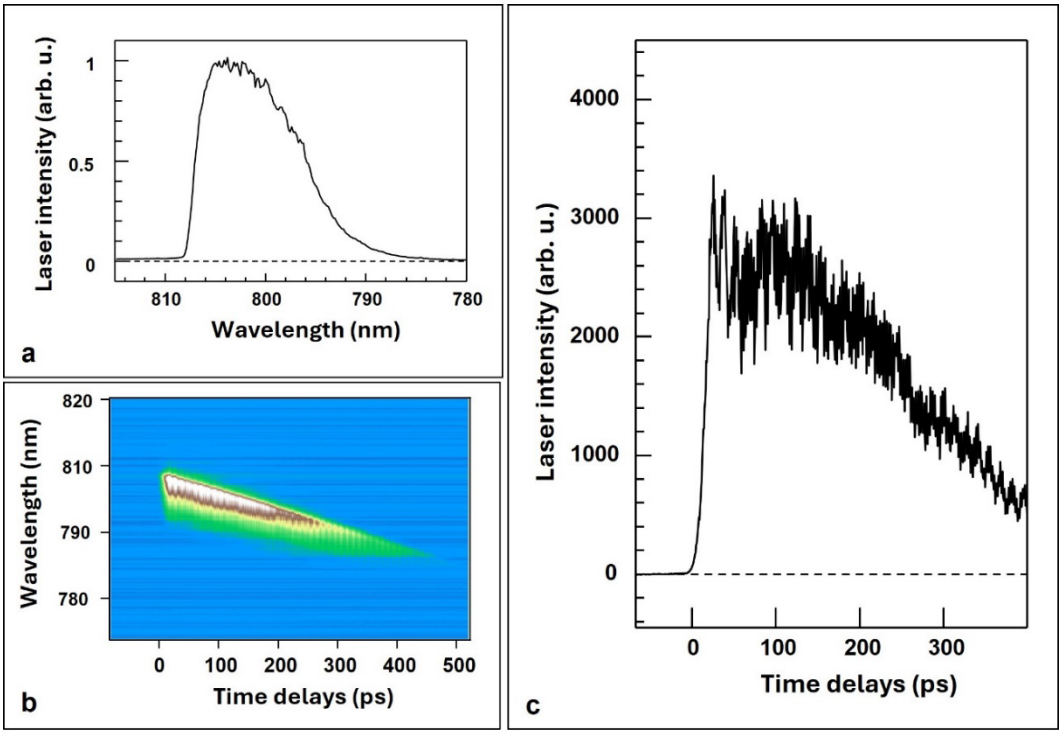

Fig. 14 Analyses of cross-correlation frequency-resolved optical gating of a chirped laser pulse used to generate steady heat pulse sustained for more than 500 ps. a) spectrally shaped chirped laser spectrum, which is sharply cut in the lower frequencies to generate sharp rise of the heat pulse, b) 2D scan of cross-correlation wavelength-resolved optical gating used to map out the laser wavelength in time, c) laser intensity over all wavelengths as a function of time.

We are also interested in the polarization dependency of heat transfer in explosives. In general, for a crystal sample or an orderly oriented sample with large dipole moments, maximum absorption occurs when the molecules are parallel to the polarized probing light. Conversely, minimum absorption is observed when the molecules are perpendicular to the polarized probing light. Based on the rule of polarized light absorption in orderly oriented samples, we have developed polarization-resolved UV-VIS TA spectroscopy coupled with our ultrafast indirect laser heating technique to investigate the transient orientation of polar molecules due to the transient thermal gradient generated by the heat propagation in a liquid and the dependence of the energy coupling on orientations of solid sample. Investigations were made of transient orientations of nitromethane and polarization dependency of heat energy coupling into RDX molecules, and the results were reported in Dang et al.[15] Using our current technique, we can observe the transient orientation of large dipole molecules occurring in picosecond and sub-picosecond time scales due to the thermal gradient and the orientation dependency of heat energy coupling into molecules of crystal samples.

3.6 Probing Chemical Properties

Changes in the electronic structure of the excited states have been observed experimentally via TA in shock-induced reactions.[18–21] However, questions arose as to whether the changes are caused by shock wave energy or thermal energy from T-jump during the shock loading, or both. If thermal energy contributes to the changes, does it happen before or during the chemical reactions? We have used ultrafast heating below the decomposition threshold of explosives to observe any changes in electronic configurations and determine the effect of thermal energy transfer to RDX prior to the onset of irreversible decomposition reactions.

We have investigated how and how fast thermal energy from a T-jump interacts with explosives.[10,15,16] One of the most important findings in these studies is that chemistry occurs due to the thermal energy coupling into explosive molecules via changing electronic configurations of the molecules. And the event happens before any chemical reaction occurs (as confirmed by the fact that the TA was reproducible at the same sample location). A mechanism of electronic excitation following ultrafast heating has been proposed to explain our observations. A femtosecond laser pulse interrogating a metal film will provide a tremendous energy density in the metal and a T-jump with a rate of approximately 10^{14} K/s. Under these extreme conditions, a thermal and temperature "wave" can be generated and propagate through the metal film,[12,13] resulting in severe thermal stress on the samples. Thermally induced perturbations on the electronic structure could lead to a reduction in energy band gaps, increasing the likelihood that electrons from the ground state could be promoted by the rapid heating energy. In an effort to verify the proposed mechanism, we investigated the excited states of TATB in DMSO via ultrafast heat pulses and compared the results to those obtained using optical pump-probe TA spectroscopy.[16] The comparison confirmed that under heating, electronic excitation of TATB molecules occurred at lower energy levels compared to those of the optical pump. The TATB energy bandgaps are reduced under the perturbation of the heat energy.

UV-VIS TA spectroscopy, while useful for observing electronic excitations in explosives, is less so for investigating the effects of thermal energy on a particular bond or functional group since TA spectral features are broad and not well-resolved. A possible solution is to use ultrafast MIR TA spectroscopy to monitor the molecular vibrations of materials. Furthermore, Au does not give any TA signal in the MIR region. MIR TA spectroscopy coupled with our indirect laser heating technique could be used to monitor specific chemical bonds/functional groups under rapid heating.

To observe the importance of temperature preceding and during the chemistry it drives, time-resolved single-shot MIR TA spectroscopy of explosives under long and steady heat pulse with durations of hundreds of picoseconds is the ideal experimental tool. Most importantly, the data obtained from these experiments are comparable to those obtained in ultrafast laser shock experiments in which shock energy is sustained for approximately 250 ps, and chemistry begins to occur at approximately 100 ps as observed with UV-VIS and MIR TA spectroscopies.[19–23]

Efforts have been made to address this challenge. We are currently developing a single-shot picosecond, time-resolved MIR TA spectroscopy experiment coupled with a nanosecond heat pulse. The experimental setup and data acquisition method are similar to that described in Fig. 4, except the probing WL light and the compressed laser pulse used for heating will be replaced with a MIR probe and a chirped laser pulse. To replace the probing WL, the 800-nm laser pulse will be coupled to a commercial optical parametric amplifier to generate the MIR light. The MIR light can also be generated by four-wave mixing through filamentation in air.[22–24]

Currently, we have set up an experiment to obtain the heat pulse with the desired duration. A chirped laser pulse stretched out approximately 250 ps (center at 800 nm) is used to interact with a 110-nm Au layer, successfully generating a heat pulse that is sustained for more than 1 ns. For the experimental purpose of observing time evolutions of chemistry and chemical reactions that are comparable to those obtained in ultrafast shock experiments, we have successfully generated a heat pulse that is steady at approximately 100 ps and sustains for more than 500 ps. Figure 14a shows a spectrum of the chirped laser pulse, which is spectrally shaped by sharply cutting lower frequencies of the spectrum using razor-edge at the Fourier plane of the stretcher to generate a sharp rise of the heat pulse. Figure 14b shows a 2D cross-correlation wavelength-resolved optical gating scan used to map out the laser wavelength in time, while Fig. 14c is the profile of the laser intensity across all wavelengths as a function of time. Figure 15 depicts a heat pulse generated by the chirped laser pulse in which the steady heat pulse started at approximately 100 ps and was sustained beyond 500 ps. Using this heating pulse coupled with time-resolved MIR TA spectroscopy, we will be able to investigate the importance of temperature preceding and during the chemistry it drives. Most importantly, the results obtained in the investigation are comparable to those obtained from the ultrafast laser shock experiments; therefore, they will provide more accurate information on the roles of T-jump in the shock-induced initiation of explosives.

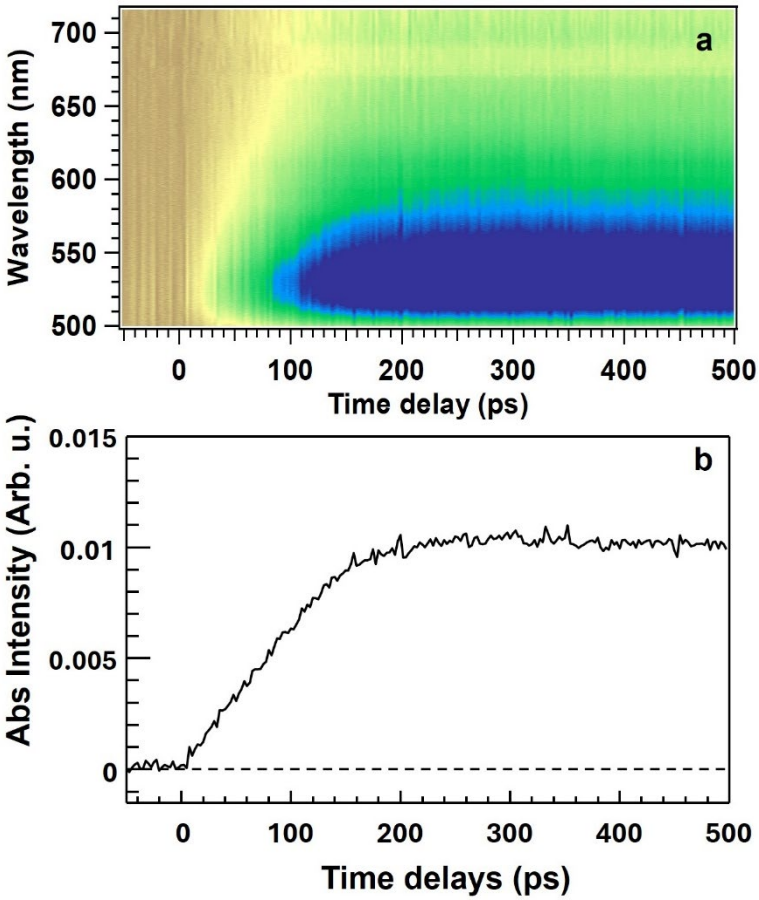

Fig. 15 a) Time-resolved transient absorption of 110-nm Au film under heating of the chirped laser pulse (spectrally shaped as shown in Fig. 14) with an energy density of 25 mJ cm^{-2}. b) Time-resolved UV-VIS transient absorption intensity profile at 525 nm of 110-nm Au film heated by the chirped laser pulse with an energy density of 25 mJ cm^{-2}.

4. Concluding Remarks

Understanding the initial events of shocked explosive materials is crucial in predicting, and potentially tailoring, shock sensitivity and performance. These features are relevant to safety and the design of explosives—essential missions of the US Army Combat Capabilities Development Command Army Research Laboratory and DOD. We have been building and developing state-of-the-art experimental capabilities, which are essential tools for investigating the roles of T-jump and its behaviors in explosives under ultrafast heating on a picosecond time scale. We have systematically investigated physical and chemical properties of explosives to determine the key factors that are involved in the initial events of a shock-induced initiation. The findings from these investigations provide essential knowledge but can also improve current techniques and develop new experimental tools for future studies. The goal is to experimentally elucidate the mechanisms for shock-induced initiation, thus reducing the reliance on numerous assumptions.

5. References

1. Dremin AN. Shock discontinuity zone effect: the main factor in the explosive decomposition detonation process. Phil Trans R Soc Lond A. 1992;339(1654):355–364.
2. Gilman JJ. Chemical reactions at detonation fronts in solids. Phil Mag B. 1995;71(6):1057–1068.
3. Dlott DD. New developments in the physical chemistry of shock compression. Ann Rev Phys Chem. 2011;62(1):575–597.
4. Brill TB, Brush PJ, James KJ, Shepherd JE, Pfeiffer KJ. T-Jump/FT-IR spectroscopy: a new entry into the rapid, isothermal pyrolysis chemistry of solids and liquids. Appl Spectrosc. 1992;46(16):900–911.
5. Kim ES, Lee HS, Mallery CF, Thynell ST. Thermal decomposition studies of energetic materials using confined rapid thermolysis/FTIR spectroscopy. Combustion and Flame. 1997;110(1-2):239–255.
6. Zhou L, Piekiel N, Chowdhury S, Zachariah MR. T-Jump/time-of-flight mass spectrometry for time-resolved analysis of energetic materials. Rapid Commun Mass Spectrom. 2009;23(1):194–202.
7. Carter JA, Wang ZH, Fujiwara H, Dlott DD. Ultrafast excitation of molecular adsorbates on flash-heated gold surfaces. J Phys Chem A. 2009;113(44):12105–12114.
8. Berg CM, Lagutchev A, Dlott DD. Probing of molecular adsorbates on Au surfaces with large-amplitude temperature jumps. J Appl Phys. 2013;113(18):183509–183520.
9. Lou T, Lloyd J R. Non-equilibrium molecular dynamics study of thermal energy transport in Au–SAM–Au junctions. Int J Heat Mass Tran. 2010;53(1–3):1–11.
10. Dang NC, Gottfried JL, De Lucia FC Jr. Energetic material response to ultrafast indirect laser heating. Appl Opt. 2017;56(3):B85–B91.
11. Maurer MJ, Thompson HA. Non-fourier effects at high heat flux. J Heat Trans-Trans-T ASME. 1973;95(2):284–286.
12. Xiong Q, Tian X. Thermomechanical interaction in metal films during ultrashort laser heating. MAMS. 2015;22(7):548–555.

13. Gan Y, Chen J K. Thermomechanical wave propagation in gold films induced by ultrashort laser pulses. Mechanics of Materials. 2010;42(4):491–501.

14. Dang NC, Gottfried JL, De Lucia FC Jr. The initial response of energetic materials in the first 50 picoseconds. Proceedings for the Sixteenth International Detonation Symposium; 2018.

15. Dang NC, Gottfried JL, De Lucia FC Jr. The responses of energetic materials under indirect ultrafast heating: polarization dependence of heat transfer in materials. Army Research Laboratory (US); 2023 Aug. Report No.: ARL-TR-9730.

16. Dang NC, Gottfried JL, De Lucia FC Jr. The electronic excitation of 2,4,6-triamino-1,3,5-trinitrobenzene in DMSO solution under indirect ultrafast heating: a comparison to results obtained by optical pumped method. DEVCOM Army Research Laboratory (US); 2023 Sep. Report No.: ARL-TR-9773.

17. Hohlfeld J, Wellershoff SS, Gudde J, Conrad U, Jahnke V, Matthias E. Electron and lattice dynamics following optical excitation of metals. Chem Phys. 2000;251:237–258.

18. McGrane SD, Moore DS, Funk DJ. Shock induced reaction observed via ultrafast infrared absorption in poly(vinyl nitrate) films. J Phys Chem A. 2004;108(43):9342–9347.

19. Dang NC, Bolme CA, Moore DS, McGrane SD. Shock induced chemistry in liquids studied with ultrafast dynamic ellipsometry and visible transient absorption spectroscopy. J Phys Chem A. 2012;116(42):10301–10309.

20. Brown KE, Bolme CA, Moore DS, McGrane SD. Ultrafast chemical reactions in shocked nitromethane probed with dynamic ellipsometry and transient absorption spectroscopy. J Phys Chem A. 2014;118(14):2559–2567.

21. Brown KE, Bolme CA, Moore DS, McGrane SD. Ultrafast shock-induced chemistry in carbon disulfide probed with dynamic ellipsometry and transient absorption spectroscopy. J Appl Phys. 2015;117(8):085903.

22. Bowlan P, Powell M, Perriot R, Martinez E, Kober EM, Cawkwell MJ, McGrane S. Probing ultrafast shock-induced chemistry in liquids using broad-band mid-infrared absorption spectroscopy. J Chem Phys. 2019;150 (20):204503.

23. Powell MS, Bowlan PR, Son SF, Bolme CA, Brown KE, Moore DS, McGrane SD. A benchtop shock physics laboratory: ultrafast laser driven shock spectroscopy and interferometry methods. Rev Sci Instrum. 2019;90(6):063001.

24. Fuji T, Suzuki T. Generation of sub-two-cycle mid-infrared pulses by four-wave mixing through filamentation in air. Opt Lett. 2007;32(22):3330–3332.

List of Symbols, Abbreviations, and Acronyms

Δt	propagation time
Au	gold
CCD	charge-coupled device
DMSO	dimethyl sulfoxide
DOD	Department of Defense
HMX	octahydro-1,3,5,7-tetranitro-1,3,5,7-tetrazocine
MIR	mid-infrared
PETN	pentaerythritol tetranitrate
Pt	platinum
RDX	1,3,5-trinitroperhydro-1,3,5-triazine
SAM	self-assembled monolayer
Si	silicon
T_e	electron temperature
T_l	lattice temperature
T-jump	temperature jump
TA	transient absorption
TATB	2,4,6-triamino-1,3,5-trinitrobenzene
UV-VIS	ultraviolet-visible
WL	white light

1 (PDF)	DEFENSE TECHNICAL INFORMATION CTR DTIC OCA
1 (PDF)	DEVCOM ARL FCDD RLB CI TECH LIB